MUMT 618: Week #11

1 Bowed String Modeling

The modeling of string instruments was covered earlier in this course. However, a discussion of the bowing mechanism was delayed because of its inherent non-linearity. As we'll see here, there are some similarities between model approximations for the clarinet reed and the bowed string mechanism [McIntyre et al., 1983].

1.1 The String Model

- As previously discussed, wave propagation along a string of finite length can be efficiently and accurately modeled with digital waveguide techniques.
- The "nut" is assumed ideally rigid, resulting in a reflection coefficient of -1 for displacement or velocity wave components.
- The bridge is assumed to have a finite impedance, so that some energy is transferred from the string to the instrument body.
- Several recent studies [Mansour et al., 2016b, Maestre et al., 2015] have reported results of using two-dimensional measured bridge admittance and radiativity to derive accurate body filter designs for use in simulations.
- Losses along the string cause the string energy to decay (in the absence of a driving mechanism). The losses can be commuted and implemented at discrete positions along the distributed string model.
- When bowed, the string is effectively split into two sections, one on either side of the bow. Thus, damping filters must be derived for each of the two string sections. In Mansour et al. [2016b,a, 2017], measurements of string damping were fit to a theoretical model reported by Valette [1995] (representing viscous effect of the surrounding air, viscoelasticity and thermoelasticity of the string material, and internal friction) and then used to design corresponding digital filters.
- The effects of dispersion resulting from string stiffness are less audible in bowed string instruments because a driven system is forced to vibrate periodically. However, the natural inharmonicity of the strings will "color" the resulting harmonic sound spectrum, as well as have some influence on the bow-string interaction.
- An efficient dispersion filter design method was reported by Abel and Smith [2006] and used by Mansour et al. [2016b] to model dispersion in the two string segments.
- Note that such filters must be re-designed if the bow position changes, making the task of accurate, flexible and efficient modeling of bowed-string damping and dispersion extremely difficult.
- A bowed-string model reported in Mansour et al. [2016a] included two transverse, as well as torsional, dimensions of wave propagation.

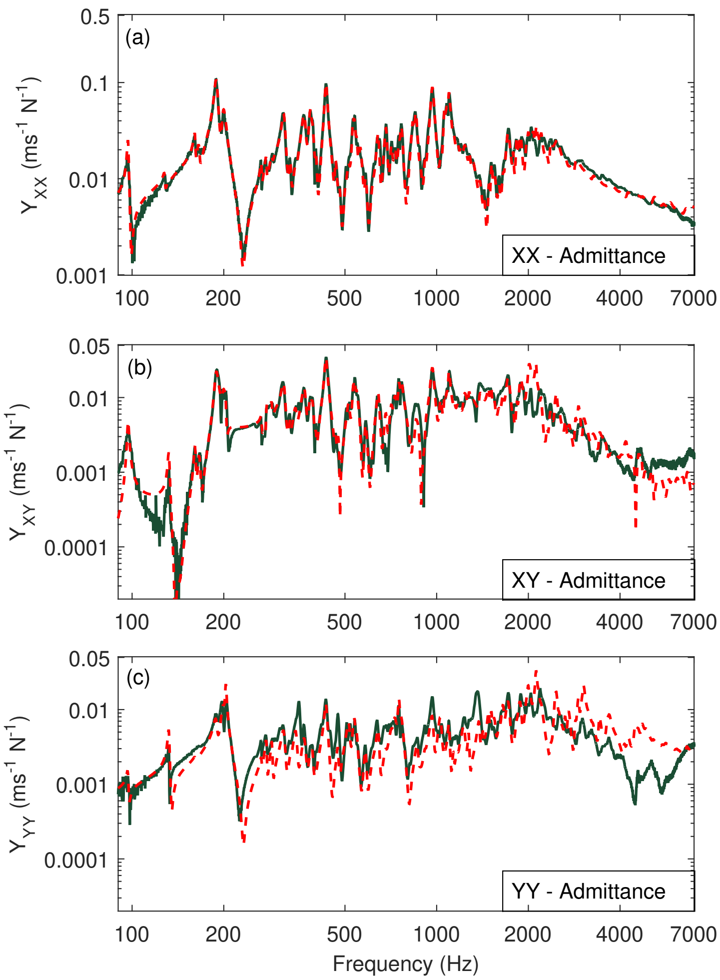

Figure 1: Measured and fit cello admittances (from Mansour et al. [2016b]).

1.2 The Bowing Mechanism

- Under normal, ideal bowing conditions, the bow and string interaction is referred to as a "stick-slip" mechanism: During the greater part of each vibration, the string is "stuck" to the bow and is carried with it in its motion. Then the string suddenly detaches itself and moves rapidly backward until it is caught again by the moving bow.
- The beginning and end of the slipping are triggered by the arrival of the propagating bend or "kink".
- This behavior of the bowed string is referred to as "Helmholtz motion."
- The string's vertical displacement at any one point is given by an unsymmetric triangular pattern (but at the string's midpoint, it is symmetric).
- The round-trip time depends only on the string length and the wave velocity.
- This mechanism allows the player to add energy to the string and to sustain its vibrations.
- Bowing near the string end requires greater force and produces a louder, brighter sound than bowing farther from the end.
- The amplitude of vibration can be increased either by increasing the bow speed or by bowing closer to the bridge.

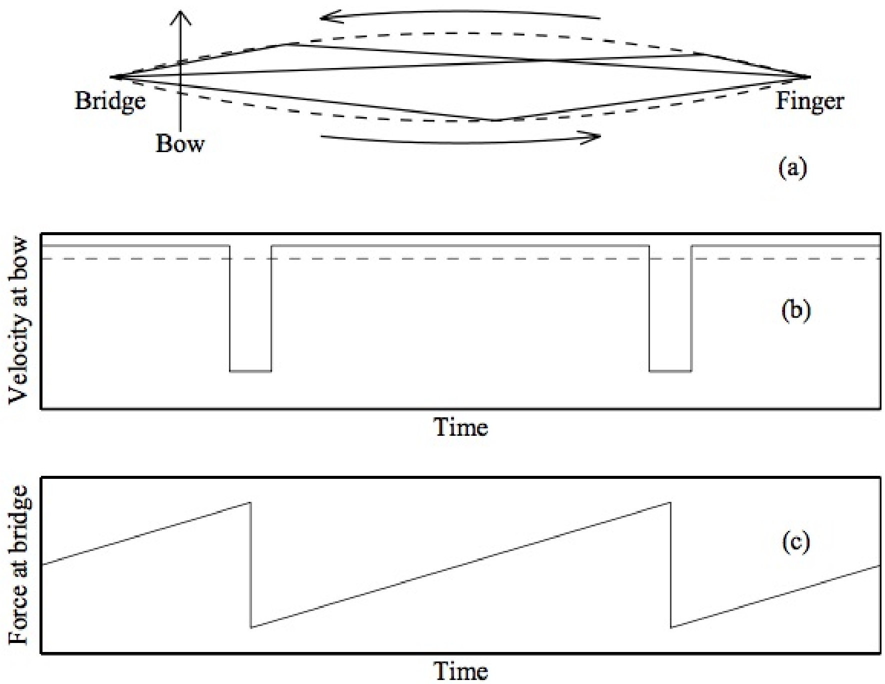

Figure 2: Idealized version of the Helmholtz motion of a bowed string: (a) sketch of the string displacement at three points in the vibration cycle (with exaggerated vertical scale); (b) waveform of string velocity at the bow-string contact point; (c) waveform of transverse force exerted on the violin bridge (from Woodhouse [2014]).

- The violinist has a limited parameter space within which to work, governed by minimum and maximum bow forces that vary according to the position along the string, as depicted in Fig. 3.

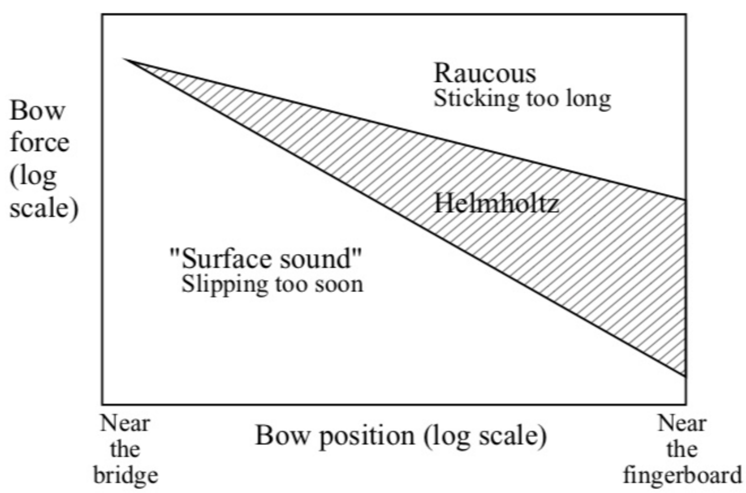

Figure 3: Sketch of a Schelleng diagram [Schelleng, 1973], showing the region of the bow force / bow position plane within which it is possible to sustain a steady Helmholtz motion of the string (from Woodhouse [2014]).

1.3 The Bow-String Interaction

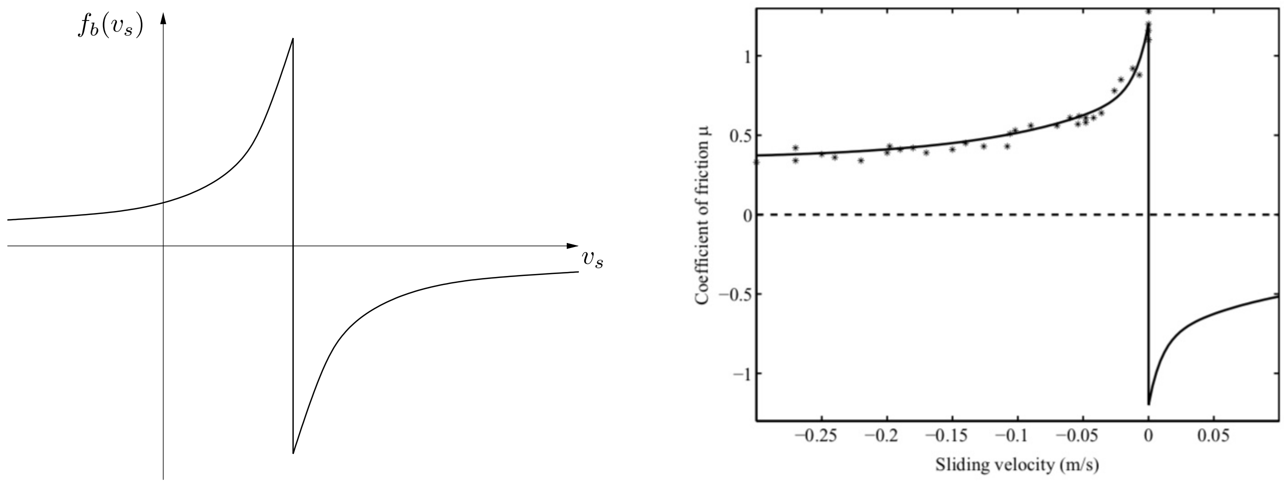

Figure 4: (left) Friction force exerted on string by the bow; (right) Modeled friction coefficient from measured data (from Woodhouse [2014]).

- An approximation to the friction force exerted by the bow on the string is shown in Fig. 4 [Friedlander, 1953, Keller, 1953]. The curve is antisymmetric because bowing can happen in two opposite directions. This force is dependent on $v_\Delta = v_b - v_s$, the difference between the bow and string velocities.
- The bow and string are stuck together for $v_\Delta = 0$ (the point of infinite slope in the figure). In this case, the friction force is based primarily on static friction.
- For $|v_\Delta| > 0$, the string is "slipping" and the friction force is based roughly on kinetic friction, which is significantly less than the static friction (especially when rosin is applied to the bow).
- The maximum friction force is roughly proportional to the normal force between the bow and string.
- At all times, the force applied by the bow on the string must balance the reactive force of the string.
- The reactive force can be expressed in terms of the string wave impedance and traveling-wave components of velocity as $f_s = R_s[v_s^+ - v_s^-] = R_s[v_s - 2v_s^-]$, where R_s is the string wave impedance.
- A graphical solution can be found by plotting this expression together with the friction force expression to determine a resulting outgoing traveling-wave component, as shown in Fig. 5.

1.4 Simulation Results

- Figure 6 provides a few examples of simulated string force (at bridge) and velocity (at bow) waveforms. The model allows some torsional motion of the string, so the velocity of the string's centre-line need not be exactly constant during sticking: the string can roll on the sticking bow.
- An example of a simulated Schelleng diagram is shown in Fig. 7 (from Mansour et al. [2016a]). S-motion is similar to the Helmholtz motion in that there is a single stick and slip per nominal period, but the s-motion involves large ripples superposed on the expected sawtooth bridge force (it occurs when the bow position is close to a string nodal point). An ALF note is a musical tone with a frequency much lower than that of the first string mode and requires very precise control of the bow parameters to achieve. Decaying, double-slip and raucous regimes are omitted for clarity.

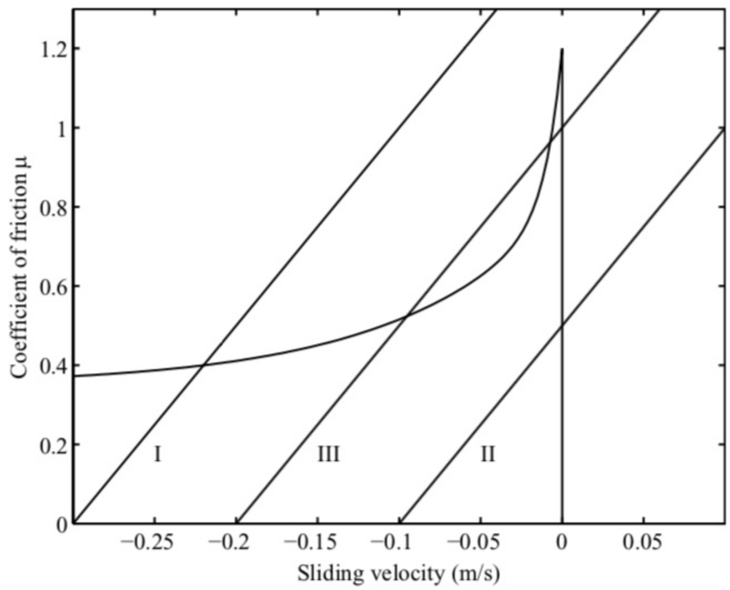

Figure 5: Friedlander graphical approach for solving the friction force and string reactive force at a given moment. Case I: sliding; II: sticking; III: case with ambiguity, resolved by a hysteresis loop (from Woodhouse [2014]).

- Other aspects of the playing behaviour can be deduced from such simulations. Figure 8 presents (a) The increase in the slip-to-stick ratio as a percentage of its theoretical value (unit x100 s/s), (b) the spectral centroid relative to the fundamental frequency (unit Hz/Hz), and (c) the pitch flattening as a percentage of the fundamental frequency (unit 100 Hz/Hz). The theoretical slopes for the minimum and maximum bow force are shown in (a) by thick diagonal lines to guide the eye (from Mansour et al. [2016a]).
- Mansour et al. [2016a] then goes on to compare the variation of these metrics with various modular model additions or subtractions, such as finger-stopping, longitudinal string vibrations, bow-stick flexibility, dual-polarisation, no torsion, no stiffness, rigid terminations, and thermal friction model.

1.5 A Digital Waveguide Scattering Approach

- The various components of the model are combined in the general system block diagram of Fig. 9.
- The bowing mechanism effectively divides the string into two parts and is implemented as a nonlinear two-port junction (in contrast to wind instrument reed mechanisms which are one-port junctions).
- As mentioned above, the applied bow force f_b must at all times balance with the reactive force of the string ($f_s = R_s[v_s^+ - v_s^-]$).
- The bow friction curve relates the bow force and the differential velocity in terms of a *friction coefficient*, $f_b(v_\Delta) = R_b(v_\Delta) \cdot v_\Delta$.
- Smith [1986] recasts the relationship in terms of a differential velocity of known, incoming junction velocities (v_Δ^+) to allow an expression of the form:

$$R_b(v_\Delta) \cdot v_\Delta = R_s \left[v_\Delta^+ - v_\Delta \right]$$

  where $v_\Delta^+ = v_b - [v_{s,l}^+ + v_{s,r}^+]$.

- Traveling-wave components entering the bow-string junction from either side have + superscripts.

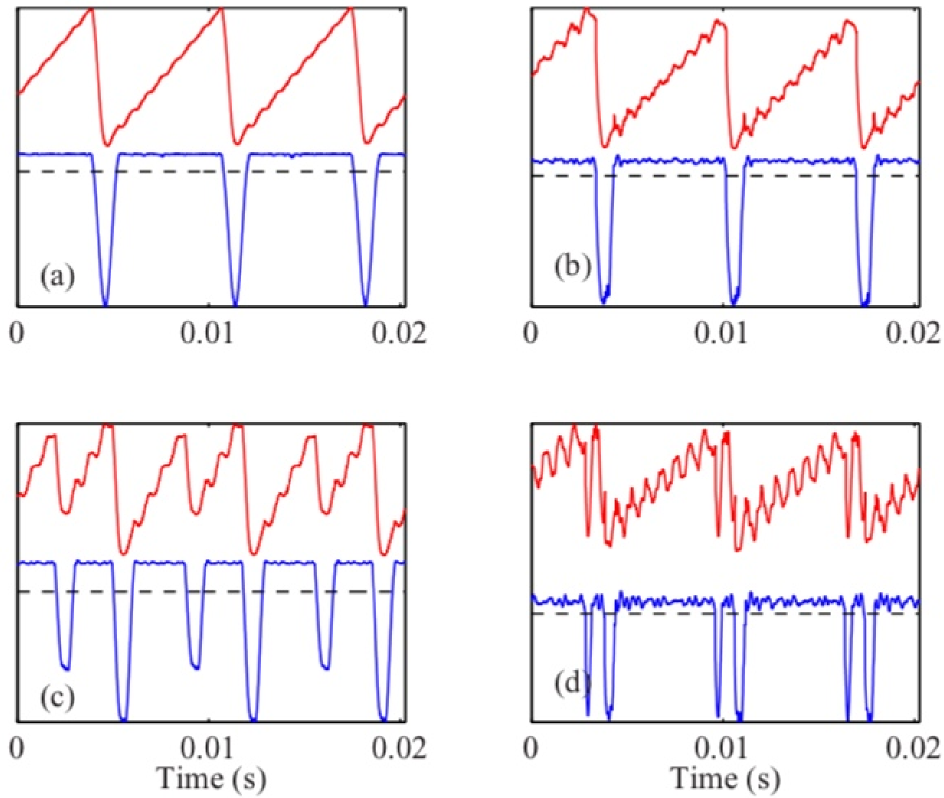

Figure 6: Simulated waveforms for a cello open D string: (a),(b) Helmholtz motion with two values of normal force; (c) Double slip motion; (d) Double flyback motion. Upper trace: bridge force (shifted vertically for clarity); lower trace: string velocity at bowed point; dashed line: zero line for velocity trace (from Woodhouse [2014]).

- Ignoring possible non-zero phase in the bow-hair dynamics, this relationship can be solved simultaneously with the friction curve and represented in terms of a memoryless reflection coefficient as:

$$\begin{aligned} v_{s,r}^- &= v_{s,l}^+ + \hat{\rho}(v_\Delta^+) \cdot v_\Delta^+ \\ v_{s,l}^- &= v_{s,r}^+ + \hat{\rho}(v_\Delta^+) \cdot v_\Delta^+ \end{aligned}$$

  where

$$\hat{\rho}(v_\Delta^+) = \frac{r(v_\Delta(v_\Delta^+))}{1 + r(v_\Delta(v_\Delta^+))}$$

  and $r(v_\Delta) = 0.25 R_b(v_\Delta)/R_s$.

- An example piece-wise linear reflection coefficient table is shown in Fig. 10.
- When the bow and string are stuck together, the velocity reflection coefficient is 1 and the $v_{s,r}^-$ and $v_{s,l}^-$ are computed so that the physical string velocity is equal to v_b.
- A velocity reflection coefficient of 0 corresponds to the absence of the bow discontinuity altogether.
- A complete digital waveguide implementation for the bowed string system, using a reflection coefficient table, is diagrammed in Fig. 11.

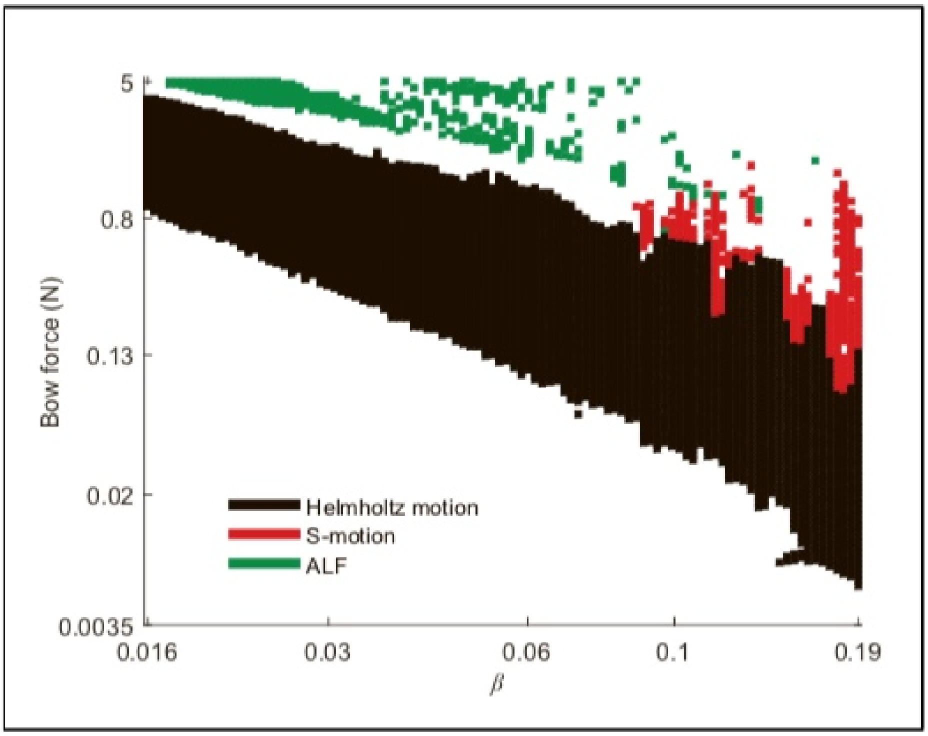

Figure 7: Simulated Schelleng diagram (from Mansour et al. [2016a]).

1.6 The Body Model

- Methods were previously discussed for modeling the string instrument body.
- A digital filter representation of a string instrument body must be of high order given the complicated nature of its spectral "signature".
- Commuted synthesis offers an efficient means for making use of a measured or synthesized body impulse response in plucked or struck string synthesis.
- Commuted synthesis, however, is possible only with linear systems.
- Julius Smith has developed a nonlinear commuted synthesis approach to bowed-string synthesis, with code examples provided.

1.7 Bowing Control

- In general, the quality of physical modeling synthesis algorithms is highly dependent on physically realistic parameter control. This is especially evident with bowed-string models.
- An interesting bowing control mechanism is reported by S. Serafin, R. Dudas, M. Wanderley, X. Rodet, *Gestural control of a real-time physical model of a bowed string instrument*. In Proceedings of the 1999 International Computer Music Conference, Bejing, China, October 1999.
- A much more refined control of the bow parameters is reported by Maestre, E., Blaauw, M., Bonada, J., Guaus, E., Pérez, A. *Statistical modeling of bowing control applied to violin sound synthesis*. IEEE Transactions on Audio, Speech, and Language Processing, Vol. 18, No. 4, pp. 855-871, 2010.

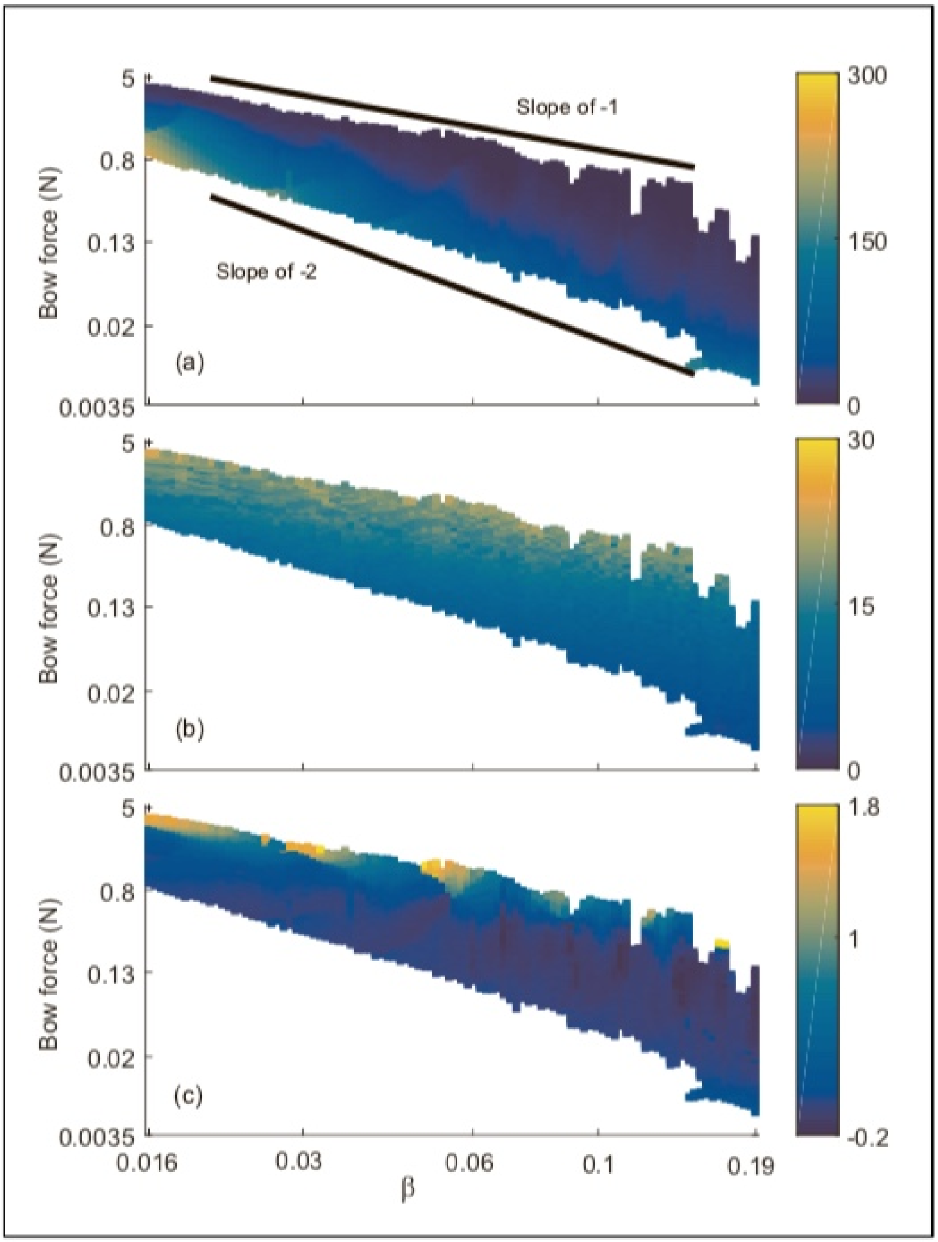

Figure 8: Simulated playing metrics (from Mansour et al. [2016a]).

2 Coupled Mode Synthesis

Coupled Mode Synthesis is a technique that was first reported by Scott van Duyne in the *Proceedings of the 1997 International Computer Music Conference* [Van Duyne, 1997]. It provides an efficient technique for modal synthesis that allows easy control over decay rates and natural coupling effects.

2.1 Traditional Modal Synthesis

- Modal synthesis is a technique that can be used to efficiently simulate the sounds of objects that exhibit a relatively small number of exponentially decaying sinusoids, such as impulsively struck bars, plates,

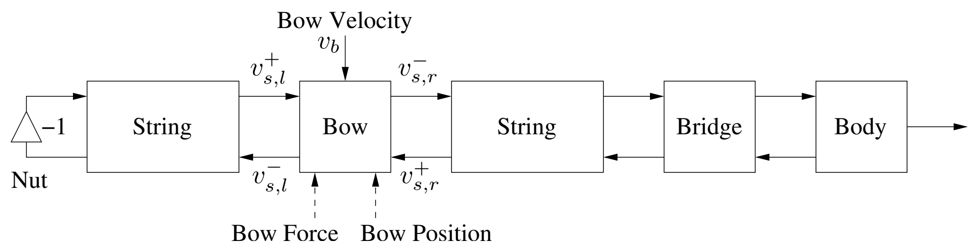

Figure 9: A bowed string system block diagram.

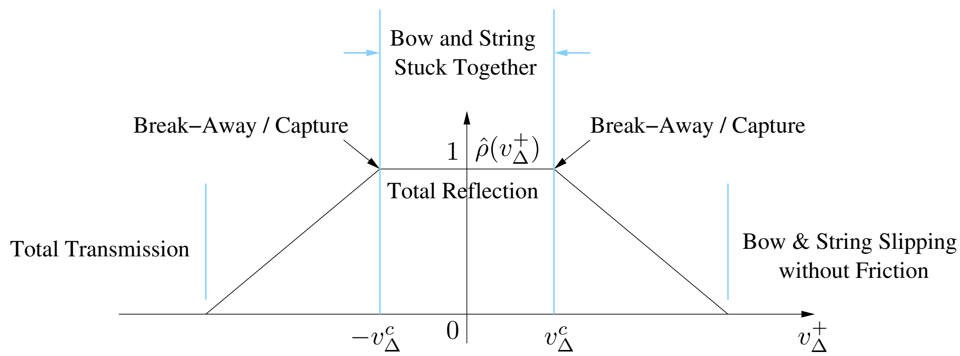

Figure 10: A bow-string reflection coefficient table.

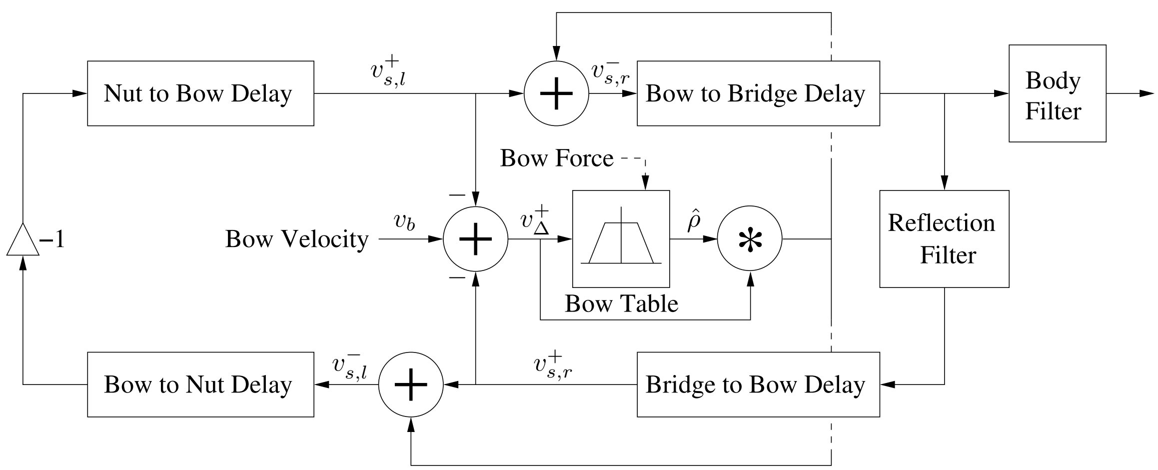

Figure 11: A complete bowed string implementation using a reflection coefficient table.

or blocks.

- These exponentially decaying sinusoids correspond to vibrating modes of the objects in question.
- In the traditional modal synthesis approach, each of these modes is modeled with a second-order digital filter of the form

$$\frac{1}{1 - 2r_k \cos(2\pi f_k T_s) z^{-1} + r_k^2 z^{-2}}, \tag{1}$$

where the f_k are the mode frequencies in Hz, the r_k are the pole radii controlling the decay rates, and T_s is the sample period.

- These resonant filters are typically connected in parallel, tuned and calibrated from measured recordings, and then excited with an appropriate "dry hit" (and/or residual) signal, as illustrated in Fig. 12.

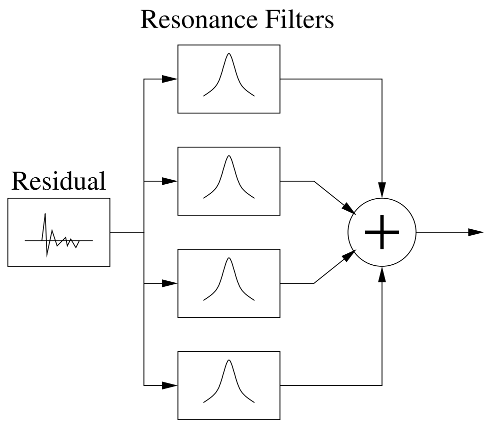

Figure 12: A traditional modal synthesis block diagram.

2.2 A Reformulation

- For reasons to be discussed in the next section, Van Duyne reformulates the second-order filter of Eq. 1 with $r_k = 1$ as

$$\frac{1}{1 + z^{-1}H_k(z)}, \tag{2}$$

where H_k is a first order allpass filter of the form

$$H_k(z) = \frac{a_k + z^{-1}}{1 + a_k z^{-1}} \tag{3}$$

and $a_k = -\cos(2\pi f_k T_s)$.

- With $r_k = 1$, the resonator does not decay but rather behaves like an oscillator with frequency f_k.
- Eq. 2 has an additional zero at $-a_k$ that is not present in Eq. 1, though this has little affect on the resonating behavior of the filter.
- A block diagram of the resulting filter structure is shown in Fig. 13.

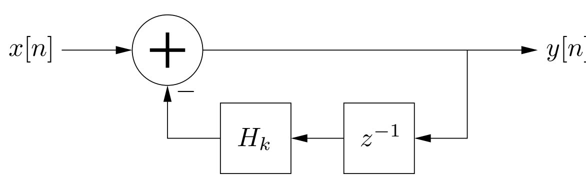

Figure 13: The CMS resonator filter structure.

2.3 Coupling the Modes

- To "couple" many modes of vibration, we can create a bank of parallel digital resonators and provide a feedback path from their summed output back to each of their inputs that is controlled by a "coupling filter".

- The filter structure of Fig. 13, however, is problematic in this context because of its direct feedforward path. If the "coupling filter" also has a direct feedforward path, the coupling structure will have a delay-free loop and not be computable.
- Van Duyne thus makes use of a modified filter structure as shown in Fig. 14.

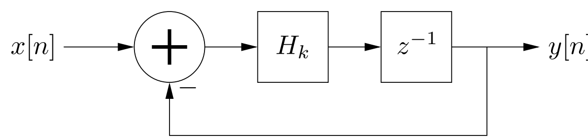

Figure 14: The modified CMS resonator filter structure.

- The filter of Fig. 14 has a transfer function given by

$$\frac{z^{-1}H_k(z)}{1+z^{-1}H_k(z)}, \tag{4}$$

- In terms of a magnitude response, the extra allpass filter H_k and unit delay z^{-1} in the numerator will have no affect. They will contribute an additional phase component but this will only modify the initial phase of the oscillations.
- With this new resonator structure, the complete coupled mode synthesis block diagram is as shown in Fig. 15.

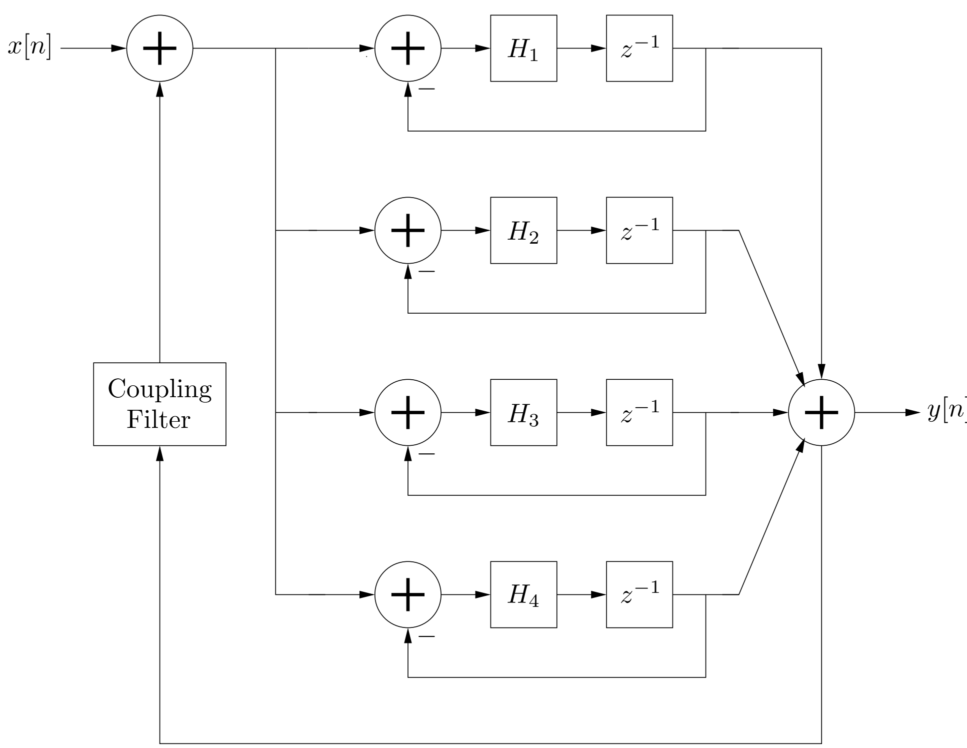

Figure 15: The coupled mode filter structure.

- Because the individual modal resonators have no attenuation, the "coupling filter" completely controls the modal decay rates.
- The "coupling filter" can be considered akin to a lumped bridge impedance. If the "bridge" is fairly rigid, only a small amount of energy from the modes will be fed back to their inputs (the "coupling filter" will typically have a magnitude response gain on the order of 0.001 or less).
- The "coupling filter" also introduces attenuation because its output is out of phase with the loop signal (the loop signal is subtracted at the loop input summer, while the input is added).
- The `cms.m` Matlab script provides an example implementation of the CMS filter structure.
- The CMS structure has a physical representation as illustrated in Fig. 16, whereby a group of mass-spring resonators are coupled via a common base which itself loses energy via a dashpot.

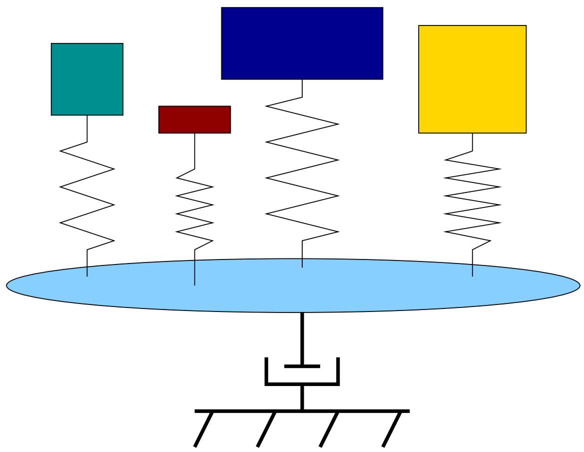

Figure 16: The CMS physical representation.

2.4 Coupling Filter Calibration

- One approach to deriving the "coupling filter" is to determine a "single mode" loop filter, $L(z)$, whose magnitude response at the various modal frequencies is equal to the respective "per sample" attenuation rates.
- The coupling filter can then be computed as

$$\frac{2\,(1 - L(z))}{1 + N + (1 - N)L(z)}, \tag{5}$$

  where N is the number of modes connected to the coupling filter.

2.5 CMS Algorithm Control

- Because the modal decay rates are controlled by a single "coupling filter", it is easy to make overall sound color modifications.
- For example, Van Duyne suggests that the "coupling filter" is naturally lowpass and that the lowpass cutoff can be modified to produce sounds that range from "wood-like" to "metalic" (in general, metal objects will have more high frequency energy).

2.6 Statistical Mode Modeling

- For sounds composed of many densely packed modes, a modeling of each mode is impractical.
- In such a case, one should choose only the most perceptually important modes to model as above. The remaining densely packed modes can then be statistically modeled using exponentially enveloped noise that is filtered by a lowpass filter whose bandwidth is decreasing over time.
- The time-varying lowpass filter causes the higher frequency energy in the noise to decay faster, a natural property in most struck percussive objects.
- A further refinement can include a strike-dependent lowpass filtering to simulate mallet brightness.
- A block diagram of the full CMS algorithm with statistical mode modeling is shown in Fig. 17.

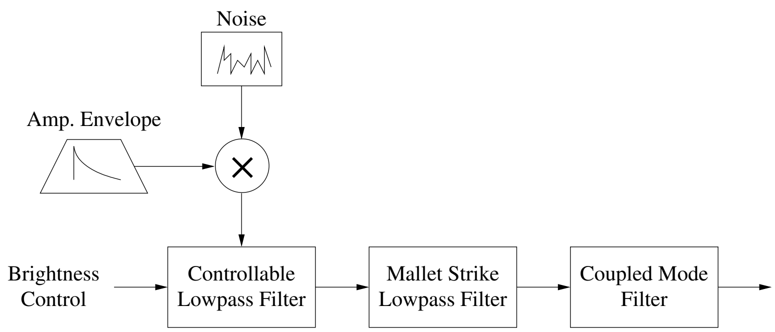

Figure 17: The CMS algorithm with statistical mode modeling.

References

J. Abel and J. Smith. Robust design of very high-order allpass dispersion filters. In *Proceedings of the 2006 International Conference on Digital Audio Effects (DAFx-06)*, pages 13–18, Montreal, Canada, 2006.

F. G. Friedlander. On the oscillations of a bowed string. In *Proceedings of the Cambridge Philosophical Society*, volume 49, pages 516–530, 1953.

J. B. Keller. Bowing of violin strings. *Comm. Pure Appl. Math*, 6:483–495, 1953.

E. Maestre, G. Scavone, and J. Smith. Digital modeling of string instrument bridge reflectance and body radiativity for sound synthesis by digital waveguides. In *Proceedings of the IEEE Workshop on Applications of Signal Processing to Audio and Acoustics*, pages 1–5, New York, Oct. 2015. IEEE Press.

H. Mansour, J. Woodhouse, and G. Scavone. Enhanced time-domain modelling of musical strings. Part 2: Bowed strings. *Acta Acustica united with Acustica*, 102:1094–1107, 2016a.

H. Mansour, J. Woodhouse, and G. Scavone. Enhanced time-domain modelling of musical strings. Part 1: Plucked strings. *Acta Acustica united with Acustica*, 102:1082–1093, 2016b.

H. Mansour, J. Woodhouse, and G. Scavone. On minimum bow force for bowed strings. *Acta Acustica united with Acustica*, 103:317–330, 2017.

M. E. McIntyre, R. T. Schumacher, and J. Woodhouse. On the oscillations of musical instruments. *Journal of the Acoustical Society of America*, 74(5):1325–1345, nov 1983.

J. Schelleng. The bowed string and the player. *Journal of the Acoustical Society of America*, 53(1):26–41, 1973.

J. O. Smith. Efficient simulation of the reed-bore and bow-string mechanisms. In *Proceedings of the 1986 International Computer Music Conference*, pages 275–280, The Hague, Netherlands, 1986. Computer Music Association.

C. Valette. *Mechanics of musical instruments*, chapter The mechanics of vibrating strings, pages 115–183. Springer-Verlag (ed. A. Hirschberg), Vienna, 1995.

S. Van Duyne. Coupled mode synthesis. In *Proceedings of the 1997 International Computer Music Conference*, pages 248–251, Thessaloniki, Greece, 1997. Computer Music Association.

J. Woodhouse. The acoustics of the violin: a review. *Reports on Progress in Physics*, 77, 2014.